Electrical field effects near the metal-insulator transition

M. Osofsky,* J. B. Bieri, M. LaMadrid, W. Contrata, and J. M. Mochel
Materials Research Laboratory, University of Illinois at Urbana-Champaign, 104 South Goodwin Avenue, Urbana, Illinois 61801
and Department of Physics, University of Illinois at Urbana-Champaign, 1110 West Green Street, Urbana, Illinois 61801
(Received 19 February 1988; revised manuscript received 19 September 1988)

A detailed study of the nonlinear conductivity of two disordered alloys, Ge_xAu_{1-x} and C_xCu_{1-x}, is carried out near their metal-insulator transition on the metallic side for 1.3 K $< T <$ 4.2 K and for electric fields E up to 500 V/cm. Analyzing the $\sigma(E)$ data in the context of an electron-gas–heating model yields unacceptably long electron relaxation times. Alternatively, the electric field can limit renormalization by pumping the electrons' energy above the disordered potential. The system then changes from quantum-mechanical scaling to classically diffusive behavior beyond a certain length scale. The temperature and electric field data can then give the characteristic lengths and prefactors for the metal-insulator transition.

Results of recent experiments[1–5] on two-dimensional systems at low temperatures have shown that dirty metals exhibit non-Ohmic dc conductivity. Anderson *et al.*[6] suggested that this behavior is the result of electrons Ohmically heating above the system's ambient temperature due to an electron-phonon bottleneck. This model implies $\tau_{e\text{-ph}}/T^{-p}$ with $0.4 \leq p \leq 2$ for several systems.[1–5] We have studied this E-field effect in three-dimensional metallic amorphous Ge_xAu_{1-x} and C_xCu_{1-x} between 1.3 and 4.2 K. Analyzing our data in the context of an electron-heating model yields long electron-phonon relaxation times and similar p's. An alternate approach, in which McMillan's[7] quantum-mechanical renormalization process is stopped when the energy an electron gains from the E field is comparable to the energy width of the disordered potential, simply describes our $\sigma(E)$ data.

We will first introduce the problem with a brief history of the effect as seen in two-dimensional systems, including the hot-electron model of Anderson *et al.* We then describe the experiment and interpret the data in the context of the electron-gas–heating model, discussing the problems with this model. Finally, we treat the phenomenon as a scaling effect and analyze the data using this novel "cutoff" in McMillan's theory.

I. INTRODUCTION

In 1979 Dolan and Osheroff[1] studied 30-Å Au-Pd films and observed a logarithmic dependence of the resistivity on E field at milliKelvin temperatures for $E \sim 0.1$ V/cm. These films had sheet resistances larger than 1000 Ω/□ at 1 K and exhibited the logarithmic temperature dependence of resistance characteristic of two-dimensional, weak-localizing systems. Bishop *et al.*[2] saw this phenomenon in their metal-oxide-semiconductor field-effect transistors (MOSFET's) at ~50 mK and $E \sim 0.001$ V/cm. Hoffmann *et al.*[3] studied the effect in 12–25 Å platinum films between 4.2 and 0.33 K at fields up to 1 V/cm. Their films had resistances of 600 to 5000 Ω at room temperature. The low-temperature conductivity increased as $0.62e^2/(2\pi^2\hbar)\ln(E)$ for high fields.[4,5]

Anderson *et al.*[6] proposed that these results are due to an electron-phonon bottleneck which introduces a thermal resistance between the localizing electrons and the phonon bath. The applied electric field would then Ohmically heat the electrons above the phonon bath. According to this model a $\sigma(E)$ experiment at a fixed temperature T is actually measuring $\sigma(T_e)$ where $T_e > T$. The difference between the electron and phonon temperatures can be calculated from a phenomenological detailed balance expression:[6]

$$P_{\text{in}} = \sigma E^2 = C\,\Delta T/\tau_{e\text{-ph}}\ , \tag{1}$$

where C is the electronic specific heat.

Bergmann[4] used magnetoconductance to measure the temperature of conduction electrons of 30-Å gold and silver films with $R \sim 130$ Ω. He found that fields of ~30 V/cm heated the conduction electrons as much as 1 K above the 4.2-K phonon bath. Using (1) he calculated a reasonable result, $\tau_{e\text{-ph}} \sim (2-3)\times 10^{-11}$ s. Dorozhkin and Dolgopolov[5] studied the effect in 50-Å gold films with $R \sim 35$ Ω between 0.4 and 4.2 K with E up to 10 V/cm. In this case sample conductivity was used to determine electron temperature and they concluded that the electrons were heating up to 15 K and thus calculated relaxation times on the order of 10^{-7} s. Similar behavior has been observed in doped germanium crystals by A. C. Anderson.[8] He measured small electron-phonon thermal impedances which varied as T,[4] like metals, and yet were insensitive to carrier concentration.

II. EXPERIMENTAL PROCEDURE

The samples consisted of 500- and 50-μm square films 30 μm apart (Fig. 1). Figure 2 shows the insert configuration. A calibrated Ge resistance thermometer was greased into a hole in the insert block which was drilled as close to the substrate as possible. The entire tip was situated in a vacuum can which was immersed in a helium bath. Helium gas could be introduced into the can via a stainless steel tube terminated with a needle

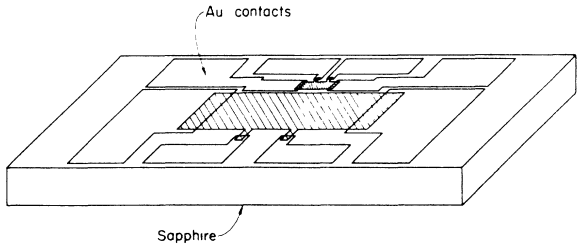

FIG. 1. The small sample is ~ 50 μm square and the large is 500 μm square. The two films are 30 μm apart with one serving as a temperature controlling thermometer for the other. The version 1 geometry is identical with the gold contacts crossing the films.

valve at the top of the insert. This configuration allowed us to control the temperature to within 1% precision.

The substrates were clamped at each end to the copper insert tip ensuring that all of the heat flowed through the ends of the substrate (Fig. 3). Indium pads between the substrate and the copper insert tip enhanced thermal contact between the substrate and insert. Teflon tape between the substrate and the retaining ring cushioned the substrate from mechanical stresses.

We used the small film as the sample, taking advantage of the small geometry to achieve large electric fields E. The large film then served as the temperature controlling thermometer. Figure 3 is a sketch of the substrate's isotherms when power is put into the sample while the can is under vacuum. The symmetry of the system, the thin substrate, and small distance between the films ensured that the sample and thermometer were at the same temperature during a measurement.

Initially, the temperature was controlled with the germanium resistance thermometer. The helium bath was

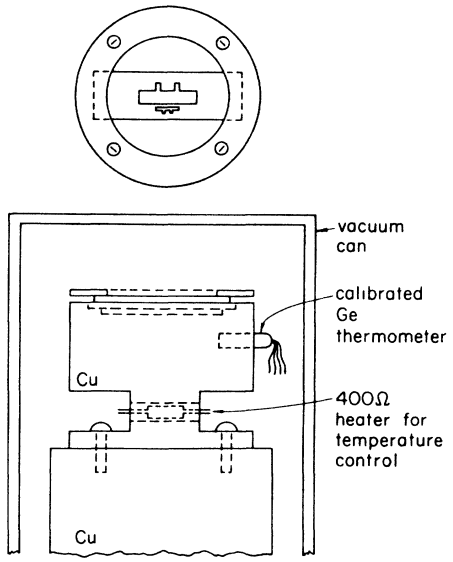

FIG. 2. Experiment insert configuration. A stainless steel tube running out of the cryostat allows the introduction of helium gas to the vacuum chamber.

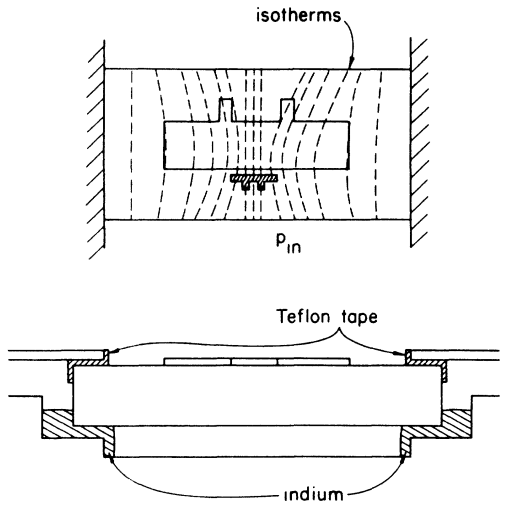

FIG. 3. Isotherm pattern of the experiment with vacuum in the sample can and current applied to the small film. The substrate is thermally anchored at both ends so heat must flow down the length of the substrate keeping the (small) sample film and (large) thermometer film at the same temperature.

pumped and the desired temperature chosen by setting the appropriate resistance on the germanium thermometer bridge with the current to the sample film turned off. When the system came to thermal equilibrium temperature control was switched to the large film thus maintaining the sample at the initial temperature as the current was increased.

Conductivity measurements were made using a four-probe method as described in earlier work[9] with the applied electric field E calculated from the measured voltage. Conductivity versus temperature measurements were made at low electric fields E for 12 K $\geq T \geq$ 1.3 K. Two sets of conductivity versus dc E-field measurements were then made: the first with the sample in vacuum and the second with a small volume of helium gas in the sam-

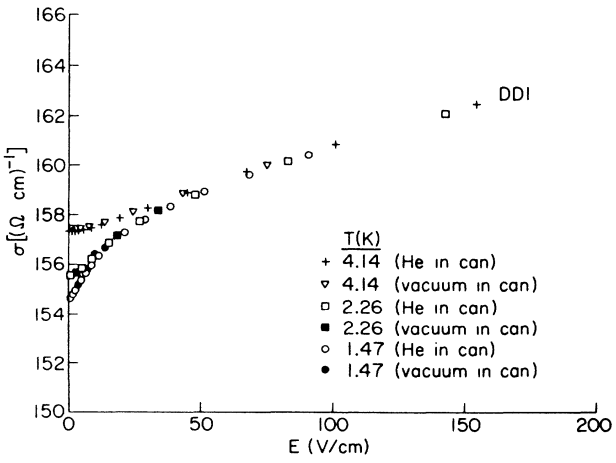

FIG. 4. Conductivity vs electric field E for sample $DD1$ (Ge-Au) at three temperatures with a vacuum in the sample can and a small volume of helium gas in the can.

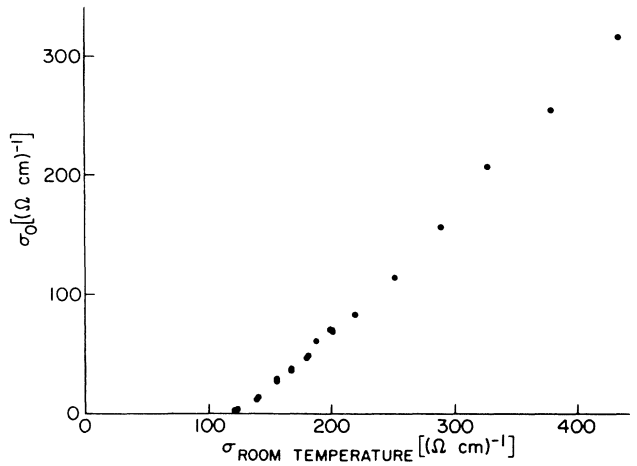

FIG. 5. Mobility edge of sputtered C-Cu. A least-squares fit finds a power law of 0.9 ± 0.2.

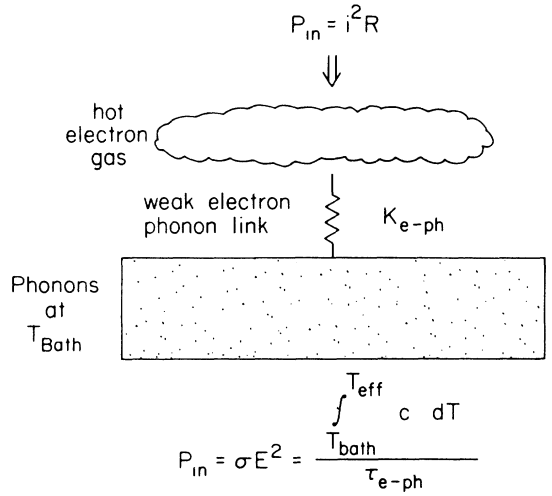

FIG. 6. The hot-electron model. An electron-phonon bottleneck produces a small thermal conductivity between the localizing electrons and the phonon bath. An applied electric field E Ohmically heats the electrons with respect to the bath and increases the conductivity as though the sample were at a warmer temperature.

ple can. The measurements with helium were necessary because in vacuum the sapphire could not carry the heat away fast enough to maintain temperature control for the highest electric fields E. The small volume of helium greatly improved the cooling power of the system by short circuiting the heat flow in the sapphire. This increase in cooling power was made at the expense of the isotherms of Fig. 3 adding some uncertainty to the sample temperature.

Figure 4 shows $\sigma(E)$ versus E data taken at three temperatures with helium gas and vacuum in the can. All of the σ versus E data fall on a single curve at high electric fields E. At low fields this curve splits into temperature-dependent branches. For each sample, the two sets of data lie on top of each other in the low-field region and into the E-field dominated regime.

The cooling power of the helium prevented film heating from interfering with E-field effects since the system remained insensitive to bath temperature at high fields. At low fields, where temperature effects dominate, any uncertainty in temperature introduced by the helium gas is negligible. Therefore, we are confident that the $\sigma(E)$ data reflects electronic behavior and not gross substrate heating.

We examined two systems, amorphous Ge_xAu_{1-x} and C_xCu_{1-x} on the metallic side of the metal-insulator transition. We reported on the characterization of Ge-Au in an earlier work.[9] Figure 5 shows the σ_0 versus $\sigma_{\text{room temp.}}$ of a series of C-Cu samples. A least-squares fit of the data to $\sigma_0 = A\,|\sigma_{\text{room temp.}} - \sigma_{\text{crit.}}|^{\nu}$ yields $\nu = 0.9\pm0.2$. Therefore, both the Ge-Au and C-Cu systems exhibit weak-localizing behavior as characterized by a mobility edge with a unity power law.

III. ELECTRON HEATING INTERPRETATION

In this section we will proceed as in previous work[1-6] and *assume* an electron-heating model. First we derive a phenomenological expression for the electron-phonon relaxation time as a function of electron temperature. Then the conductivity versus E-field data is analyzed by assum-

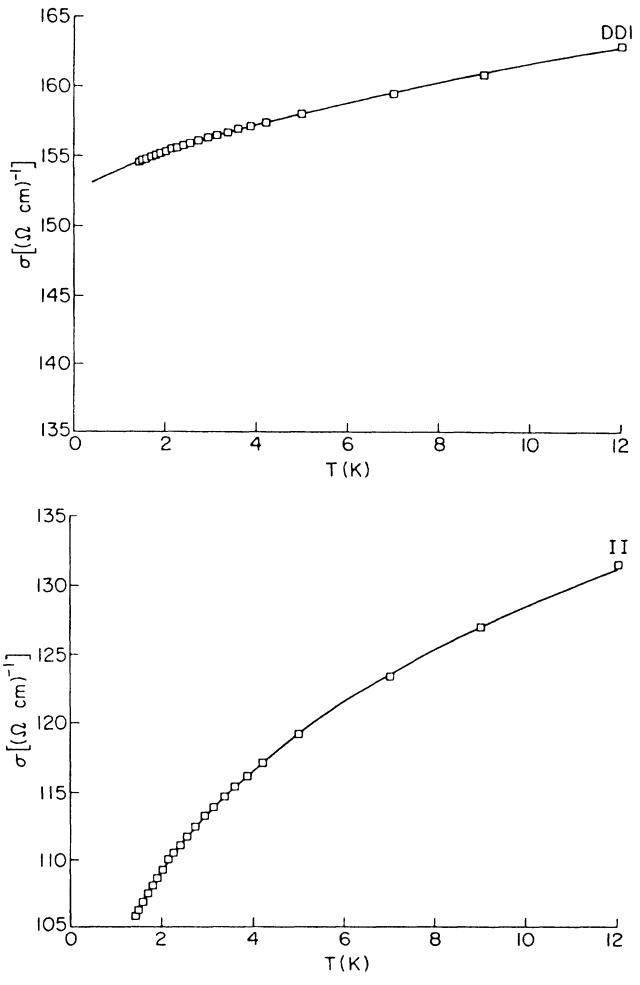

FIG. 7. Low E-field conductivity vs temperature data for samples *DD*1 (Ge-Au) and *II* (C-Cu). The lines are the best fit curves of the data to $\sigma = \sigma_0 + \sigma_1 T^{\beta}$.

ing that all of the conductivity changes were due to electron heating: finding the electron temperature from low-field conductivity versus temperature data and calculating relaxation times. The results are compared with earlier work and with estimates for normal metals.

We assume that an electron-phonon bottleneck causes the electrons to Ohmically heat with respect to the phonon bath in the presence of a large electric field E (Fig. 6). We modify the original heat balance Eq. (1) in the manner of Dorozhkin and Dolgolopov:[5]

$$\tau_{e\text{-ph}}=\frac{\int_{T_{\text{bath}}}^{T_{\text{electron}}} c\,dT}{\sigma E^2}\ , \tag{2}$$

where c is the free-electron specific heat which is given by[10]

$$c=(\pi^2/2)k_B^2 Tn/\varepsilon_F\ , \tag{3}$$

where k_B is Boltzmann's constant, T is temperature, ε_F is the Fermi energy, and n is the electron density.

Since

$$\varepsilon_F=(\hbar k_F)^2/(2m) \tag{4}$$

and

$$k_F=(3\pi^2 n)^{1/3} \tag{5}$$

we have

$$c=(\pi/3)^{2/3}k_B^2 mTn^{1/3}/\hbar^2\ . \tag{6}$$

We use the Drude conductivity expression[10] to derive an expression for n:

$$\sigma_{\text{Drude}}=\sigma_{\text{RT}}=ne^2\tau_{\text{elastic}}/m\ . \tag{7}$$

On the microscopic length, a,

TABLE I. E-field effect sample legend. Samples *GG*, *HH*, and *II* are C_xCu_{1-x} and are characterized only by their conductivity. The sample indexing provides a reference to more complete data in Ref. 9.

Sample	Material	t (Å)	Geometry	Anneal history
AA	$Ge_{0.82}Au_{0.18}$	1200	1	Room temp. for 1 d
*BB*0	$Ge_{0.78}Au_{0.22}$	1200	1	Room temp. for 1 d
*BB*1				+Room temp. for 1 month
*BB*2				+70 °C for $\frac{1}{2}$ h
*BB*3				+120 °C for 1 h
*BB*4				+150 °C for $\frac{1}{2}$ h
*BB*5				+170 °C for $\frac{1}{2}$ h
*BB*6				+190 °C for $\frac{1}{2}$ h
*BB*7				+250 °C for 1 h
CC	$Ge_{0.80}Au_{0.20}$	1800	1	Room temp. for 1 d
*DD*1	$Ge_{0.78}Au_{0.22}$	1800	1	Room temp. for 1 week
*DD*2				+85 °C for $\frac{1}{2}$ h
*DD*3				+105 °C for $\frac{1}{2}$ h
*EE*1	$Ge_{0.80}Au_{0.20}$	1700	2	Room temp. for 1 d
*EE*2				+50 °C for $\frac{1}{2}$ h
*EE*3				+110 °C for $\frac{1}{2}$ h
*EE*4				+Room temp. for 2 weeks
*FF*1	$Ge_{0.79}Au_{0.21}$	1400	2	Room temp. for 1 d
*FF*2				+50 °C for $\frac{1}{2}$ h
*FF*3				+60 °C for $\frac{1}{2}$ h
*FF*4				+70 °C for $\frac{1}{2}$ h
*FF*5				+80 °C for $\frac{1}{2}$ h
*FF*6				+90 °C for $\frac{1}{2}$ h
*FF*7				+100 °C for $\frac{1}{2}$ h
*FF*8				+110 °C for $\frac{1}{2}$ h
*FF*9				+115 °C for $\frac{1}{2}$ h
GG	C_xCu_{1-x}	3500	2	Room temp. for 1 d
HH	C_xCu_{1-x}	2000	2	Room temp. for 1 d
II	C_xCu_{1-x}	1500	2	Room temp. for 1 d

$$a = v_F \tau_{\text{elastic}} \tag{8}$$

and

$$a = 1/k_F \ . \tag{9}$$

Combining (5), (8), and (9) we get

$$\tau_{\text{elastic}} = (3\pi^2 n)^{+2/3} m/\hbar \ . \tag{10}$$

Inserting (10) into (7) and solving for $n^{1/3}$

$$n^{1/3} = \hbar(3\pi^2)^{2/3}\sigma_{\text{RT}}/e^2 \tag{11}$$

so that

$$c = [(\pi k_B/e)^2 m/\hbar]T\sigma_{\text{RT}} = \alpha\sigma_{\text{RT}}T \ . \tag{12}$$

Finally, integrating (2):

$$\tau_{e\text{-ph}} = \alpha\sigma_{\text{RT}}[(T_{\text{eff}}^2 - T_{\text{bath}}^2)/(2\sigma E^2)] \ . \tag{13}$$

Inserting the values of the constants,

$$n = (6.090\times10^{13})\sigma_{\text{RT}}^3 \ , \tag{14}$$

$$\tau_{\text{elastic}} = (5.752\times10^{-6})/\sigma_{\text{RT}}^2 \ , \tag{15}$$

$$a = (8.2158\times10^{-6})/\sigma_{\text{RT}} \ , \tag{16}$$

$$\tau_{e\text{-ph}} = (3.17\times10^{-4})\frac{\sigma_{\text{RT}}(T_{\text{eff}}^2 - T_{\text{bath}}^2)}{(2\sigma E^2)} \ . \tag{17}$$

If σ_{RT} is in $(\Omega\,\text{cm})^{-1}$ then (14) is in cm^{-3}, (15) is in s, (16) is in cm, and (17) is in s.

In analyzing the $\sigma(E)$ data we use the low-field $\sigma(T)$ data as an electron thermometer (Fig. 7). In doing this we assume all of the effect is due to electron heating and that the low-temperature conductivity is a unique measure of electron temperature. Conductivity versus temperature data were taken between 12 and 1.3 K and a 3 parameter least-squares fit of the data to $\sigma = \sigma_0 + \sigma_1 T^{\beta}$ was done. An effective temperature was calculated from

$$T_{\text{eff}} = \left[\frac{\sigma(E) - \sigma_0}{\sigma_1}\right]^{1/\beta} \tag{18}$$

for each $\sigma(E)$ data point. These values were then used in (16) to calculate the electron-phonon relaxation times.

Table I is a sample legend describing the composition, thickness, and anneal history for nine samples studied. All of the samples were $\sim 50\ \mu$m square. Figure 7 shows the $\sigma(T)$ calibration data for several runs plotted with the best fit curves. Table II presents the results of the calculations for n, a, and τ_{Drude} $(=\tau_{\text{elastic}})$. For gold[10] $n = 5.9\times10^{22}\ \text{cm}^{-3}$, $a = 1.59$ Å, and $\tau_{\text{Drude}} = 3.0\times10^{-14}$ s at 273 K and $n = 8.5\times10^{22}\ \text{cm}^{-3}$, $a = 1.41$ Å, and $\tau_{\text{Drude}} = 2.7\times10^{-14}$ s at 273 K for copper.

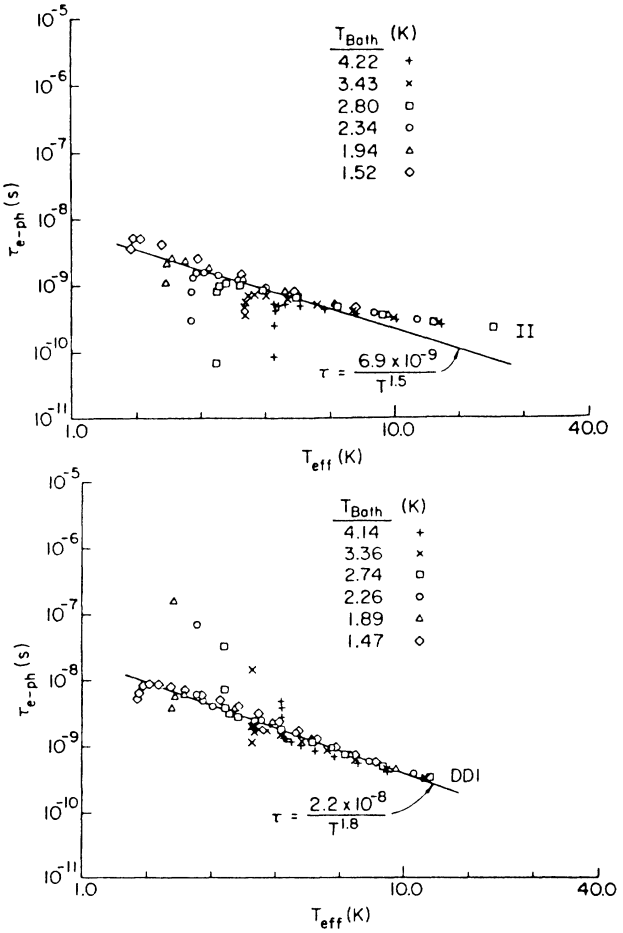

FIG. 8. Electron-phonon relaxation times vs effective temperature for samples *DD*1 (Ge-Au) and *II* (C-Cu). The times and temperatures were determined from $\sigma(E)$ data taken at several bath temperatures using the hot-electron model (see text). The line is a guide to the eye.

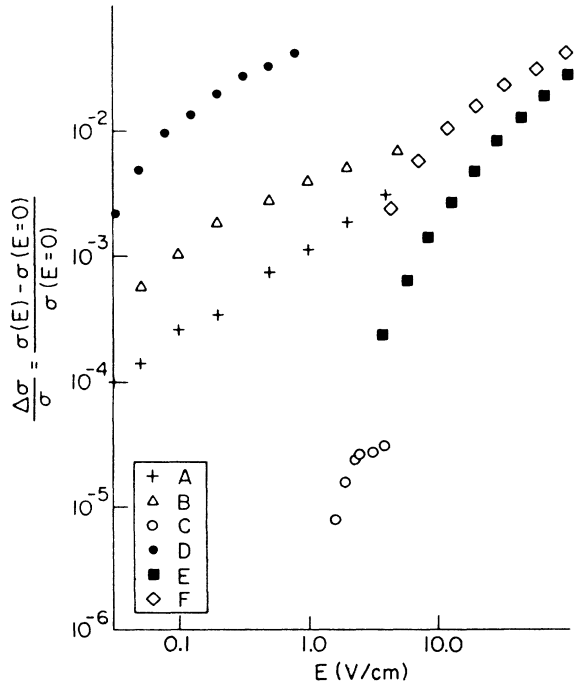

FIG. 9. Normalized change of conductivity vs E for several systems at several temperatures: *A*, 50-Å Au at 4.2 K (Dorozhkin and Dolgolopov); *B*, 50 Å Au at 0.65 K; *C*, 30 Å Au at 4.2 K (Bergmann); *D*, MOSFET at 273 mK (Dolan and Osheroff); *E*, sample *EE*4 at 4.2 K; *F*, sample *EE*4 at 1.8 K.

The electron densities calculated from the data are up to 2 orders of magnitude smaller than pure gold or copper. The microscopic lengths, a, are larger and the elastic relaxation times longer than in the pure metals. This is consistent with the samples being dilute metals.

Figure 8 shows electron-phonon relaxation times as a function of the effective temperature plotted with guides to the eye. Several features of these plots should be noted. Most of the data have $\tau_{e\text{-ph}} \sim T^{-p}$ with $1.2 \lesssim p \lesssim 1.9$. Anderson *et al.*[6] predict $\tau_{e\text{-ph}} \sim T^{-3}$ for three-dimensional systems in our temperature range. Both Dolan and Osheroff[1] and Bishop *et al.*[2] found $p \sim 2$ while expecting $p = 4$ in their two-dimensional systems at low temperatures.[6] Dorozhkin and Dolgopolov[5] found $p = 0.4$–0.8 in their two-dimensional films and analyzing Hoffmann *et al.*[3] data in a similar manner yields $p \sim 1.3$.

A second, and more significant, feature of the data is the $\sim 10^{-9}$–10^{-7} s relaxation times between 1 and 4.2 K. These results are consistent with Dorozhkin and Dolgopolov[5] who believed they saw times on the order of 10^{-7} s at 1 K. Calculating the electron-phonon relaxation time from the electrical conductivity of very clean gold yields $\sim 2 \times 10^{-10}$ s at 4.2 K. Roukes *et al.*[11] measured the electron-phonon relaxation times of 1000-Å copper films at milliKelvin temperatures using an electron noise technique. As expected, they found $\tau_{e\text{-ph}} \sim T^{-3}$. Extrapolating their results to 1 K gives $\tau_{e\text{-ph}}(1\text{ K}) \sim 1.5 \times 10^{-8}$ and $\tau_{e\text{-ph}}(4.2\text{ K}) \sim 2.1 \times 10^{-10}$. Therefore, at ~ 1 K, our (and Dorozhkin and Dolgolopov's) data intersect the gold data of Roukes *et al.* with relaxation times $\sim 10^{-8}$ s. This implies that data taken below 1 K can begin to show hot-electron effects.

Figure 9 is a plot of $\Delta\sigma/\sigma = [\sigma(E) - \sigma(E=0)]/\sigma(E=0)$ versus E extracted from the literature for several systems and for sample *EE*4. Bergmann's results (C), which imply $\sim 10^{-11}$ s relaxation times, are 1 to 2 orders-of-magnitude smaller than other measurements at 4.2 K and were probably caused by electron heating. If the other 4.2-K results were due to electron heating their $\Delta\sigma(E)/\sigma$ data would look more like Bergmann's.

The milliKelvin data shows a very large effect which strongly increases with decreasing temperature. This is due to hot-electron effects, since at those temperatures relaxation times longer than 10^{-8} s with T^{-3}–T^{-4} dependence are expected.

A hot-electron model of this behavior in our samples mandates electronic specific heats 1 to 2 orders-of-magnitude larger than in normal metals for which there is no justification at this time. As an alternative we have developed a simple scaling explanation which describes the data.

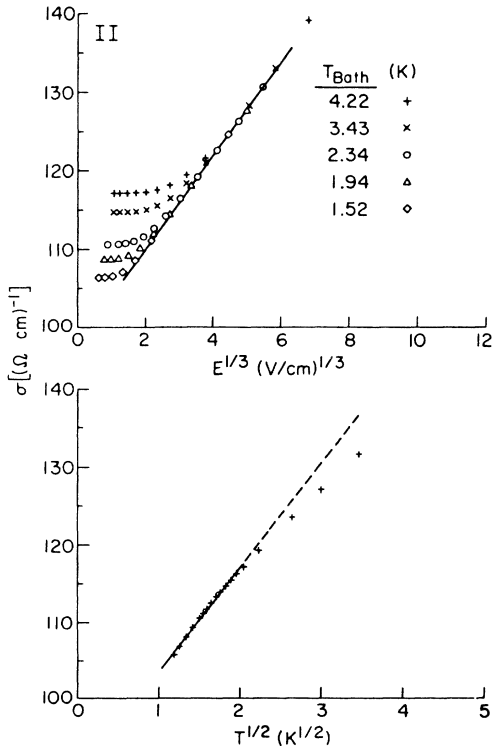

FIG. 10. Low E conductivity vs $T^{1/2}$ and conductivity vs $E^{1/3}$ data (taken at several bath temperatures) for sample *II* (C-Cu). The lines are the best fits of the data to $\sigma = \sigma_0 + \sigma_1 T^{1/2}$ and $\sigma = \sigma_0 + \sigma_2 E^{1/3}$. The maximum of the best fit $E^{1/3}$ line corresponds to the maximum of the E-field fitting range. The temperature data was fitted for $1.3\text{ K} \leq T \leq 4.2\text{ K}$.

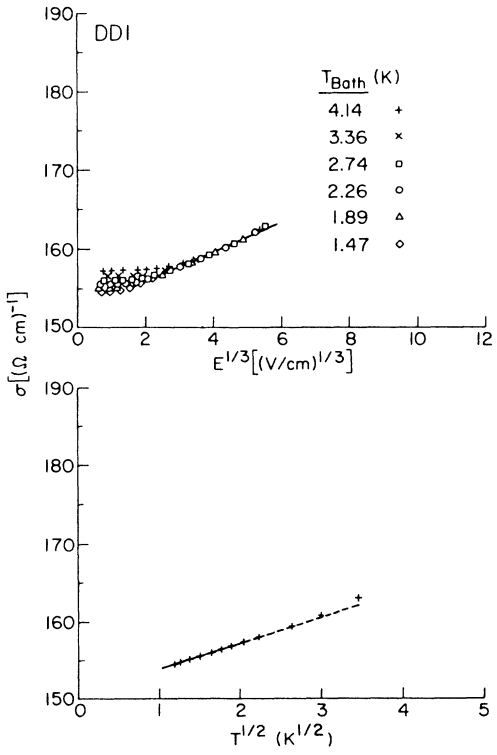

FIG. 11. Low E conductivity vs $T^{1/2}$ and conductivity vs $E^{1/3}$ data (taken at several bath temperatures) for sample *DD*1 (Ge-Au). The lines are the best fits of the data to $\sigma = \sigma_0 + \sigma_1 T^{1/2}$ and $\sigma = \sigma_0 + \sigma_2 E^{1/3}$. The maximum of the best fit $E^{1/3}$ line corresponds to the maximum of the E-field fitting range. The temperature data was fitted for $1.3\text{ K} \leq T \leq 4.2\text{ K}$.

IV. McMILLAN SCALING

In this section we examine the problem in the context of McMillan's renormalization group theory with a new type of nonequilibrium scaling cutoff. This mechanism is not an inelastic process but the effective decoupling of the electrons from the disordered potential due to the acquisition of energy from the electric field E_T.

Weakly localizing electrons elastically interact with the disordered potential until an inelastic interaction (such as electron-electron) cuts off the scaling process. Until such an event occurs the electron maintains a constant average energy since the elastic scattering is against the "lattice" of immovable ions. So far, the effect of adding energy via an electric field E has been neglected. We propose that, since a weakly localizing electron cannot lose energy until an inelastic interaction occurs, large fields raise the average energy of the electron above the disordered potential, effectively stopping scaling.

In this discussion we will assume electron-phonon relaxation times small enough to prevent hot-electron effects. The following expressions describe the normal process whereby renormalization is cut off by thermal fluctuations (electron-electron interactions). McMillan's length dependent conductivity expression for the metallic regime, modified to estimate the arbitrary prefactor, is

$$\sigma_L = \kappa[e^2/(\hbar\xi)](1+\xi/L) \tag{19}$$

with

$$L^2 = \xi^2(\Delta/F_L) \ . \tag{20}$$

Setting $F_L = k_B T$ we find

$$L_T = \xi[\Delta/(k_B T)]^{1/2} \tag{21}$$

so that

$$\sigma(T) = \kappa e^2/(\hbar\xi)[1+(k_B T/\Delta)^{1/2}] = \sigma_0 + \sigma_1 T^{1/2} \ . \tag{22}$$

We then find

TABLE II. Least-squares fit of data to $\sigma = \sigma_5 + \sigma_6 T^{\beta}$ for 1.3 K $\leq T \leq$ 4.2 K [in $(\Omega\,\mathrm{cm})^{-1}$ units].

Sample	σ_5	σ_6	β	χ^2
AA	−10±2	13±2	0.25±0.03	2.0×10^{-4}
*BB*0	340±10	10±10	0.2±0.2	5.4×10^{-3}
*BB*1	259.0±0.7	1.8±0.7	0.9±0.2	2.9
*BB*2	210±20	30±30	0.11±0.07	1.6
*BB*3	84±2	12±3	0.36±0.04	9.0×10^{-4}
*BB*4	77.9±0.9	6.1±0.9	0.42±0.04	2.8
*BB*5	73±2	6±2	0.36±0.09	7.7
*BB*6	69.4±0.7	4.8±0.7	0.34±0.04	1.0
*BB*7	68±1	3.5±1.0	0.40±0.08	4.1
CC	102±2	3±2	0.8±0.2	1.6×10^{-2}
*DD*1	150.8±0.5	3.1±0.5	0.53±0.06	2.8×10^{-4}
*DD*2	122.7±0.3	1.7±0.3	0.77±0.06	2.8
*DD*3	49.2±0.5	5.6±0.5	0.60±0.03	5.3
*EE*1	121.8±0.4	2.5±0.4	0.54±0.06	2.3×10^{-4}
*EE*2	103.1±0.2	1.0±0.1	0.89±0.06	1.6
*EE*3	−5±1	12±1	0.41±0.04	7.5
*EE*4	−5±1	11±1	0.42±0.04	9.5
*FF*1	150±20	200±50	0.02±0.07	2.0×10^{-2}
*FF*2	315±4	9±4	0.31±0.07	5.9×10^{-4}
*FF*3	283±2	7±2	0.37±0.07	7.2
*FF*4	249±2	7±1	0.39±0.05	4.1
*FF*5	193.0±0.6	3.5±0.5	0.62±0.05	5.2
*FF*6	136.0±0.3	2.1±0.2	0.88±0.04	4.1
*FF*7	100.8±0.3	2.2±0.2	0.97±0.05	8.0
*FF*8	33±2	13±2	0.49±0.04	1.3×10^{-3}
*FF*9	−13±3	26±3	0.32±0.03	1.6
GG	797±5	4±3	0.5±0.2	3.2×10^{-3}
HH	286±6	9±5	0.3±0.1	5.9×10^{-4}
II	−40±40	140±50	0.07±0.03	1.7×10^{-3}

$$\sigma_0=\kappa e^2/(\hbar\xi) \tag{23}$$

and

$$\sigma_1=\sigma_0(k_B/\Delta)^{1/2} . \tag{24}$$

Now apply an E field. At a length scale, L_E, the energy an electron gains from the electric field exceeds the uncertainty of the electron energy, F_{L_E}. Setting these two energies equal for L_E,

$$eEL_E=F_L=\Delta(\xi/L_E)^2 \tag{25}$$

so

$$L_E=\xi[\Delta/(eE\xi)]^{1/3} . \tag{26}$$

Conductivity on this length scale becomes

$$\sigma(E)=\kappa e^2/(\hbar\xi)[1+(eE\xi/\Delta)^{1/3}]=\sigma_0+\sigma_2E^{1/3} . \tag{27}$$

so that

$$\sigma_2=\sigma_0(e\xi/\Delta)^{1/3} . \tag{28}$$

Solving for Δ, ξ, κ, L_T, and L_E in terms of the experimental parameters σ_0, σ_1, and σ_2,

$$\kappa=\hbar k_B/e^3(\sigma_2^3/\sigma_1^2)=(0.354)(\sigma_2^3/\sigma_1^2) , \tag{29}$$

$$\Delta=k_B(\sigma_0/\sigma_1)^2=(8.62\times10^{-5})(\sigma_0/\sigma_1)^2 , \tag{30}$$

$$\xi=k_B/e[\sigma_2^3/(\sigma_0\sigma_1^2)]=(8618)[\sigma_2^3/(\sigma_0\sigma_1^2)] , \tag{31}$$

$$L_T=k_B/e(\sigma_2/\sigma_1)^3T^{-1/2}=(8618)(\sigma_2/\sigma_1)^3T^{-1/2} , \tag{32}$$

$$L_E=k_B/e(\sigma_2/\sigma_1)^2E^{-1/3}=(8618)(\sigma_2/\sigma_1)^2E^{-1/3} , \tag{33}$$

for E in V/cm. The lengths are in angstroms and the energy is in electron volts. A similar analysis yields identical expressions for L_T and L_E when the system is in the critical regime when $L\leq\xi$.

TABLE III. Least-squares fit of data to $\sigma=\sigma_3+\sigma_4E^{\gamma}$ for $0\leq\sigma\leq\sigma_{\max}$ [in $(\Omega\,\mathrm{cm})^{-1}$ and V/cm units].

Sample	$\sigma_{\max}$	σ_3	σ_4	γ	χ^2
AA	15.2	1.05±0.7	1.2±0.3	0.39±0.03	1.5×10^{-2}
*BB*0	358	348±4	3±2	0.31±0.09	5.0×10^{-2}
*BB*1	280	257.8±0.6	4.4±0.5	0.27±0.06	1.1
*BB*2	259	247.5±0.8	2.7±0.6	0.35±0.04	1.1
*BB*3	121	96±2	2.7±0.5	0.40±0.04	1.6×10^{-1}
*BB*4	101	83.9±0.3	1.1±0.1	0.48±0.02	1.5×10^{-2}
*BB*5	92	80.5±0.8	0.3±0.2	0.62±0.09	3.5
*BB*6	85	74.5±0.5	0.4±0.2	0.55±0.07	3.0
*BB*7	82	71.6±0.6	0.6±0.2	0.54±0.05	1.5
CC	119	105.0±0.5	1.9±0.5	0.37±0.04	1.6×10^{-2}
*DD*1	166	153.9±0.4	0.8±0.3	0.47±0.04	2.1×10^{-2}
*DD*2	138	124.6±0.4	0.6±0.1	0.53±0.04	2.4
*DD*3	79	52.3±0.5	2.6±0.2	0.38±0.04	1.2
*EE*1	127	124.7±0.1	0.46±0.05	0.56±0.02	3.8×10^{-3}
*EE*2	116	104.5±0.5	0.33±0.15	0.63±0.06	1.6×10^{-2}
*EE*3	31	2.1±0.8	3.0±0.4	0.36±0.02	1.6×10^{-1}
*EE*4	32	4±2	2.3±0.8	0.40±0.04	1.9 ± 10^{-2}
*FF*1	387	375±4	2±1	0.37±0.06	2.3×10^{-1}
*FF*2	337	326.6±0.6	0.7±0.3	0.53±0.05	9.4×10^{-3}
*FF*3	304	290±1	2.3±0.9	0.34±0.05	6.2×10^{-2}
*FF*4	270	256.7±0.6	1.3±0.3	0.43±0.04	1.5
*FF*5	212	195.8±0.8	1.7±0.4	0.41±0.04	2.9
*FF*6	159	137.9±0.5	1.6±0.2	0.46±0.02	3.6
*FF*7	128	99.9±0.7	2.8±0.4	0.39±0.02	1.6
*FF*8	81	41.2±0.9	5.8±0.6	0.32±0.01	5.0×10^{-3}
*FF*9	51	4±3	8±2	0.27±0.02	2.1×10^{-1}
GG	814	800.8±0.4	2.2±0.3	0.45±0.04	1.2×10^{-2}
HH	307	294.8±0.4	0.8±0.1	0.54±0.1	2.8×10^{-3}
II	136	99.7±0.8	5.0±0.5	0.36±0.01	8.4 ± 10^{-3}

TABLE IV. Least-squares fit of data to $\sigma=\sigma_0^T+\sigma_1 T$ for $1.3\ \text{K}\le T\le 4.2\ \text{K}$ [in $(\Omega\,\text{cm})^{-1}$ units].

Sample	σ_0^T	σ_1	χ^2
AA	−2.1±0.1	4.93±0.09	2.7×10^{-3}
*BB*0	345.7±0.2	3.5±0.1	6.5×10^{-3}
*BB*1	256.0±0.2	4.4±0.1	5.4
*BB*2	242.6±0.2	4.9±0.1	7.5
*BB*3	88.6±0.1	7.76±0.08	2.7
*BB*4	79.29±0.04	4.77±0.04	5.0×10^{-4}
*BB*5	75.4±0.1	3.57±0.06	1.1×10^{-3}
*BB*6	71.58±0.05	2.78±0.03	4.0×10^{-4}
*BB*7	68.91±0.06	2.50±0.04	4.8
CC	98.4±0.4	5.8±0.2	2.0×10^{-2}
*DD*1	150.52±0.05	3.35±0.03	2.9×10^{-4}
*DD*2	120.8±0.1	3.46±0.07	1.6×10^{-3}
*DD*3	47.28±0.08	7.36±0.05	1.4
*EE*1	121.51±0.04	2.78±0.03	2.4×10^{-4}
*EE*2	101.3±0.1	2.63±0.07	1.9×10^{-3}
*EE*3	−2.39±0.09	8.79±0.06	1.6
*EE*4	−2.61±0.04	8.77±0.03	1.5
*FF*1	367.9±0.5	5.8±0.4	5.1×10^{-2}
*FF*2	319.4±0.1	477±0.07	2.1×10^{-3}
*FF*3	285.6±0.1	4.85±0.06	1.2
*FF*4	251.45±0.07	4.84±0.05	8.6×10^{-4}
*FF*5	191.52±0.08	4.80±0.05	9.7
*FF*6	133.3±0.3	5.2±0.1	6.5×10^{-3}
*FF*7	95.8±0.3	6.6±0.2	1.6×10^{-2}
*FF*8	33.64±0.09	12.16±0.08	1.3×10^{-3}
*FF*9	−0.5±0.3	13.8±0.2	1.1×10^{-2}
GG	796.9±0.1	3.79±0.09	3.0×10^{-3}
HH	290.5±0.1	3.98±0.08	2.1×10^{-3}
II	90.0±0.6	13.4±0.4	5.6×10^{-2}

We computed least-squares fit of our high E-field data to $\sigma(E)=\sigma_0^E+\sigma_2 E^{1/3}$ and $\sigma(E)=\sigma_3+\sigma_4 E^{\gamma}$ and the temperature data to $\sigma(T)=\sigma_0^T+\sigma_1 T^{1/2}$ and $\sigma(T)=\sigma_5+\sigma_6 T^{\beta}$. Figures 10 and 11 show $\sigma(T)$ versus $T^{1/2}$ and $\sigma(E)$ versus $E^{1/3}$ plots with best fit lines.

Much of the $\sigma(T)$ data exhibit $T^{1/2}$ behavior at low T and power laws larger than $\frac{1}{2}$ at high T which has led us to traditionally cut our temperature data fits off at $T=4.2$ K. The anomalous high-temperature data is probably due to sample morphology (on the short length scales these temperatures probe) and electron-phonon interactions cutting off the diffusion process.

Power laws weaker than $\frac{1}{2}$ are either due to sample morphology or two-dimensional effects. True two-dimensional systems are described by $\sigma = A\ln(T/T_0)$. Fitting the data for these weak power law samples to $\sigma=\sigma_0+A\ln(T/T_0)$ yields larger χ^2's than power law fits indicating that the samples are not two dimensional. However, this behavior may be due to the systems crossing over from three- to two-dimensional behavior.

Choosing the fitting range for the $\sigma(E)$ data is more difficult. In addition to morphology problems we must also deal with points breaking from the universal curve at the crossover to temperature dominated behavior, a downward bend in the data at low E which is present in several samples and true hot-electron effects at the highest fields.

The choice of fitting range must minimize the influence of such features on the fit. There was no way to objectively choose a low-field limit for the data. Points which broke, either horizontally (due to crossover) or vertically, from the universal curves as determined by eye were excised. At high electric fields E, data which corresponded to effective temperatures larger than 16 K as calculated in Sec. III were eliminated. This criterion was motivated by results exemplified by Fig. 8. Most of the $\tau_{e\text{-ph}}$ versus T_{eff} curves bend towards the horizontal at $T_{\text{eff}}\sim 16$ K and $\tau_{e\text{-ph}}\sim 10^{-10}$ s. Since such relaxation times are reasonable in a real system, we interpret the bends to signify the onset of hot-electron effects and reject those points from the fits. Varying the range of the data (both the upper and lower limits) and observing the effect on the fitting parameters shows that no relevant information is lost by applying these criteria.

Tables II–V show the results of the fits. Figure 12 is a plot of the E-field power law, γ versus σ_0. About half of the γ's are $\sim\frac{1}{3}$ and about half are larger. The average is 0.43±0.10. The β's are quite spread out with an average of 0.5±0.3. Figure 13 shows that $\sigma_0^T\sim\sigma_0^E$ as is required by this nonequilibrium scaling model.

We can calculate the values of the parameters of Eqs. (29)–(33) from the extracted values of σ_0, σ_1, and σ_2. Table VI shows the results of these calculations as

$$L_E = AE^{-1/3} \tag{34}$$

and

$$L_T = BT^{-1/2}\ . \tag{35}$$

McMillan's prefactor, κ, becomes 0.4±0.2. The values of ξ range from 6 to ~2000 Å and the temperature and E-field dependent coherence lengths are on the order of 100 to 1000 Å.

V. DISCUSSION AND CONCLUSIONS

The deviations from $T^{1/2}$ and $E^{1/3}$ conductivity behaviors reflect the fact that the theory's assumption of uniform disorder is not realized on all length scales. Conductivity measurements on real systems often deviate from the predicted behavior.[9]

McMillan estimated a κ on the order of 0.1 which is consistent with the value calculated above. Magnetoresistance data yield inelastic scattering times[12] of $\sim 10^{-12}$–10^{-13} s and typical diffusivities[12] of ~1–100 cm^2/s giving typical coherence lengths of ~10–1000 Å which agree with the lengths calculated above. The values of Δ and the scaling with σ_0^2 (Fig. 14) are consistent with McMillan's predictions and the tunneling results of McMillan,[13] Hertel *et al.*,[14] Cochrane and

TABLE V. Least-squares fit of data to $\sigma=\sigma_0^E+\sigma_2 E$ for $0\le\sigma\le\sigma_{max}$ [in $(\Omega\,\mathrm{cm})^{-1}$ and V/cm units].

Sample	σ_{max}	σ_0^E	σ_2	χ^2
AA	15.2	−0.5±0.1	1.90±0.02	1.7×10^{-2}
*BB*0	358	348.0±0.3	2.9±0.1	4.9×10^{-2}
*BB*1	280	259.7±0.6	2.91±0.04	2.4
*BB*2	259	247.1±0.2	2.99±0.05	1.1
*BB*3	121	93.2±0.3	4.23±0.07	1.9×10^{-1}
*BB*4	101	80.1±0.3	3.06±0.06	9.2×10^{-2}
*BB*5	92	76.3±0.7	2.2±0.1	1.4×10^{-1}
*BB*6	85	71.8±0.3	1.82±0.08	7.6×10^{-2}
*BB*7	82	68.4±0.4	2.21±0.08	5.4
CC	119	104.5±0.2	2.37±0.07	1.6×10^{-1}
*DD*1	166	152.2±0.2	1.86±0.05	3.8×10^{-2}
*DD*2	138	121.9±0.3	2.19±0.08	9.5
*DD*3	79	50.3±0.2	3.73±0.04	3.0
*EE*1	127	122.4±0.3	1.81±0.06	5.6×10^{-2}
*EE*2	116	100.3±0.4	2.24±0.08	6.2
*EE*3	31	0.7±0.2	3.75±0.04	2.0×10^{-1}
*EE*4	32	1.1±0.4	3.60±0.08	2.1
*FF*1	387	374.6±0.4	2.1±0.1	1.9×10^{-1}
*FF*2	337	323.3±0.3	2.39±0.08	3.0
*FF*3	304	289.7±0.2	2.40±0.07	6.0×10^{-2}
*FF*4	270	254.8±0.2	2.52±0.06	3.0
*FF*5	212	194.1±0.2	2.81±0.06	4.7
*FF*6	159	134.5±0.5	3.54±0.08	1.4×10^{-1}
*FF*7	128	97.2±0.2	4.31±0.05	3.5×10^{-2}
*FF*8	81	42.3±0.1	5.22±0.02	5.8×10^{-3}
*FF*9	51	9.0±0.4	5.21±0.08	2.7×10^{-1}
GG	814	799.1±0.2	3.68±0.09	3.1×10^{-2}
HH	307	290.6±0.2	2.95±0.07	2.6×10^{-2}
II	136	98.1±0.2	5.97±0.04	1.2×10^{-2}

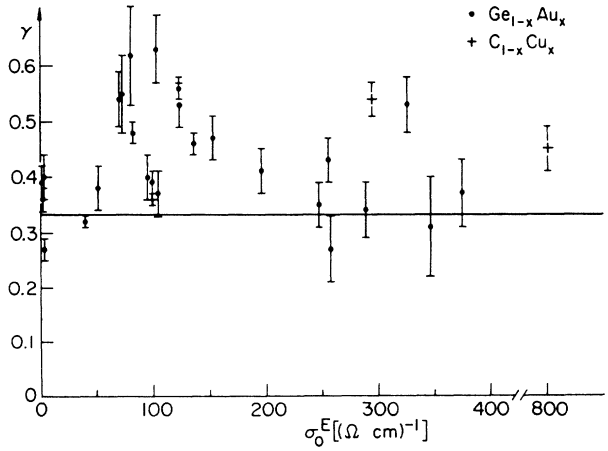

FIG. 12. The E-field power law, γ, vs σ_0^E.

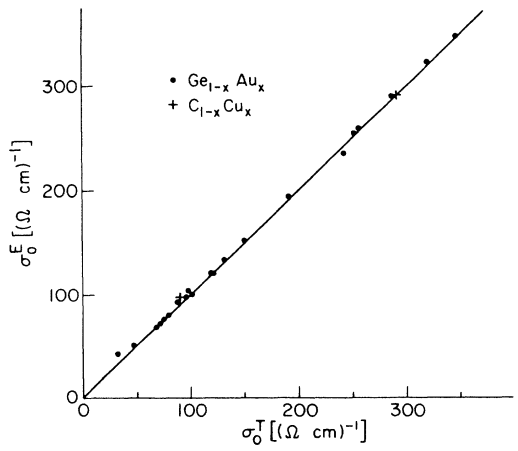

FIG. 13. Plot of σ_0^E vs σ_0^T.

TABLE VI. McMillan parameters calculated from Eqs. (29)–(33) (in Å, V/cm, and eV units).

Sample	κ	ζ	A	B	Δ
AA	0.10±0.01		1270±50	490±30	$10^{-5}\pm10^{-5}$
*BB*0	0.71±0.08	50±6	5900±500	4900±700	0.85±0.05
*BB*1	0.45±0.03	43±3	3770±200	2500±200	0.30±0.01
*BB*2	0.39±0.03	39±3	3210±170	1960±150	0.215±0.009
*BB*3	0.45±0.02	119±7	2560±100	1400±80	0.012±0.001
*BB*4	0.45±0.03	136±8	3550±150	2280±150	0.024±0.001
*BB*5	0.30±0.04	95±13	3270±320	2020±290	0.039±0.002
*BB*6	0.28±0.04	94±13	3690±330	2420±330	0.057±0.001
*BB*7	0.61±0.07	217±25	6730±530	5950±710	0.065±0.002
CC	0.14±0.02	34±4	1440±130	580±80	0.026±0.003
*DD*1	0.20±0.02	33±3	2660±150	1470±130	0.176±0.004
*DD*2	0.31±0.04	62±7	3450±290	2190±270	0.106±0.004
*DD*3	0.34±0.01	168±9	2210±60	1120±40	$(3.8\pm0.3)\times10^{-3}$
*EE*1	0.27±0.03	54±5	3650±250	2380±250	0.166±0.004
*EE*2	0.58±0.07	139±17	6250±560	5320±710	0.126±0.007
*EE*3	0.24±0.01		1570±40	669±25	$10^{-6}\pm10^{-6}$
*EE*4	0.22±0.01		1450±60	596±35	$10^{-7}\pm10^{-7}$
*FF*1	0.10±0.02	6±1	1130±190	400±100	0.35±0.05
*FF*2	0.21±0.02	16±2	2160±160	1080±120	0.39±0.01
*FF*3	0.21±0.02	16±2	2110±130	1040±99	0.304±0.009
*FF*4	0.24±0.02	23±2	2340±120	1220±90	0.235±0.006
*FF*5	0.34±0.02	43±3	2950±140	1730±120	0.139±0.004
*FF*6	0.58±0.05	106±8	3990±240	2720±230	0.057±0.002
*FF*7	0.65±0.05	154±12	3670±240	2400±230	0.018±0.001
*FF*8	0.34±0.01	218±23	1590±20	682±16	$(8\pm2)\times10^{-4}$
*FF*9	0.26±0.01	2000±2000	1230±50	460±30	$10^{-5}\pm10^{-5}$
GG	1.2±0.1	37±3	8120±550	7890±810	3.8±0.2
HH	0.57±0.05	48±4	4730±290	3510±330	0.46±0.02
II	0.42±0.03	109±8	1710±100	760±70	$(4.2\pm0.4)10^{-3}$

Strom-Olsen,[15] and Lesueur *et al.*[16]

Earlier scaling explanations[17,18] of the E-field effect were met with objections based on the argument that a dc electric field does not break time-reversal symmetry and therefore cannot delocalize electrons.[4,19] While breaking time-reversal symmetry certainly delocalizes electrons, nothing precludes other delocalizing mechanisms. Furthermore, this argument is made within linear-response theory for arbitrarily small, slowly varying E. All of the terms in the expansion which would cause these nonlinear effects are thrown out due to their complexity so the analysis self-consistently prohibits an E-field effect.[20]

We should also point out that Kaveh *et al.* and Mott and Kaveh[18] deduced an $E^{1/3}$ correction to conductivity by introducing a new cut-off length, L_E', putting $eEL_E' \sim \hbar/\tau_i$. However, the E field cannot cut off the renormalization in the same manner as inelastic interactions because the electric field E has no characteristic interaction time. Such times are necessary to impose an uncertainty on the electron energy. The electric field only increases the electron's energy. This "inelastic" E-field cutoff is not equivalent to the one derived above.

We can gain some insight by realizing that the electron wave-packet energy smear is on the order of the energy smear of the disordered potential on the same length scale. This follows from McMillan's[7] use of Abrahams *et al.*[21] dimensionless conductance, $g_L = F_L/E_L = V_L/W_L$ [Fig. 15(a)] where E_L is the average spacing of the electron wave-packet energy levels, V_L is the energy smear of the random potential, and W_L is the average of the random potential of a block of material with sides of length L. By setting $F_L = eEL$ we say the electron gains an amount of energy which is comparable to the energy smear of the potential, making these fluctuations less important and stopping further renormalization, i.e., the electrons decouple from the potential. Thus $\sigma(E)$, the measured conductivity, is very close to σ_{L_E}. Figure 15(b) shows F_L which is $\sim V_L$, and D_L, the length scale dependent diffusivity, as a function of length scale. Renormal-

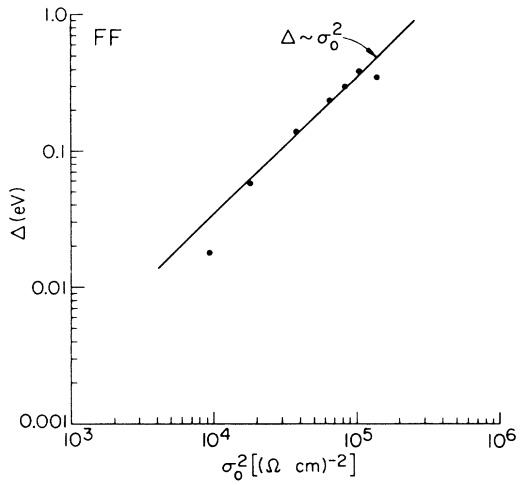

FIG. 14. Plot of Δ vs σ_0^2 for sample *FF*. The result is consistent with $\Delta \sim \sigma_0^2$ as predicted by McMillan and observed by others (see text).

ization proceeds until $F_L \sim eEL$ which occurs at length $L = L_E$. On length scales longer than L_E, but shorter than the inelastic scattering length, the system is in a steady state with length independent properties (i.e., diffusivity, conductivity, etc.). The system can be described as classically diffusing particles, so-called diffusons, which are eventually destroyed by inelastic interactions. Again, this model assumes that the electron-phonon relaxation time is short enough to prevent Ohmic heating. As the temperature of the system decreases and the relaxation time increases we expect hot-electron effects to modify, and finally dominate, the $\sigma(E)$ behavior.

It is tempting to interpret this nonequilibrium process as electron heating. In the hot-electron model the E field adds energy to the system but the bottleneck is between the electrons and the phonon bath. The electrons inelastically interact, cutting off renormalization and thermalizing the energy gained from the field keeping them in thermal equilibrium with each other.

In our scaling model the electrons, by virtue of the renormalization process, are isolated from each other and energy gained from the field cannot be thermalized until an elastic interaction occurs. The "bottleneck" is between the electrons. When the inelastic event occurs the environment, i.e., the phonon bath, thermalizes the excess energy.

Several questions invite further study. We have provided a phenomenological model which describes the system's behavior and quantifies the parameters of the renormalization group. However, there is no microscopic model of the phenomenon. These results will remain in question until a microscopic justification for our model is accomplished and direct measurements of the electron temperature are made.

Recently Fu[22] has considered a model for electric field enhancement of the conductivity through current noise production within a coherence volume. The application of a large dc electric field times the fundamental fluctuations of conductivity produce a local ac current which in turn disrupts phase coherence leading to an enhanced dc conductivity. This indirect effect on the conductivity follows an $E^{1/3}$ dependence, but the model predicts an effect ten times smaller than observed. Fu's model depends critically on the density of tunneling states within a coherence volume, which can only be estimated. In principle this noise could be measured experimentally but would require probing a single coherence volume in a three-dimensional metal insulator.

The problem could also be resolved by a theory which could account for anomalously large electronic heat capacities. Attempts at electronic specific heat measurements are difficult since it will be impossible to separate from other linear contributions found in a disordered metal. Usually the low-temperature specific heats of disordered

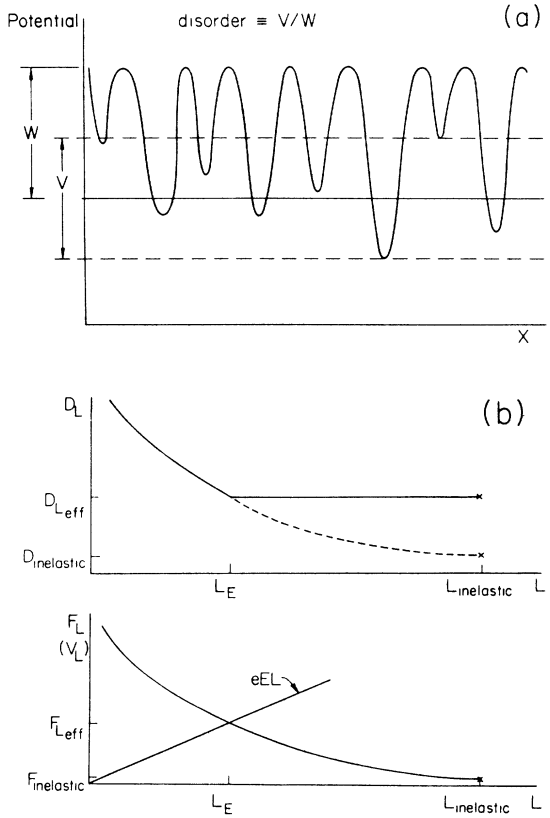

FIG. 15. (a) The Anderson potential. Disorder is defined as V/W where W is the average depth of the disordered potential and V is the mean-square deviation of the potential from the mean. (b) Intuitive, real space, picture of the scaling model. In the absence of an E field the renormalization process continues until an inelastic event occurs. Since the electrons only undergo elastic interactions with a lattice which effectively has infinite mass, an applied electric field E increases the electrons kinetic energy. The energy width of the wave packet, F_L, is on the order of the mean-square deviation of the potential from the mean, V_L. Therefore, when the energy increase is on the order of the energy width of the wave packet the system decouples from the disorder. Scaling stops, i.e., D becomes a constant, and the system classically diffuses until an inelastic interaction destroys the packet.

metals are larger than those of normal metals and most of the difference can be attributed to disordered lattice and tunneling state contributions.

At the time of this writing all attempts to independently measure the electron temperature have failed. The most promising were Johnson noise measurements similar to the work of Roukes *et al.*[11] on copper. However, our systems exhibit strong $(1/f)$-like noise behavior into megaHertz frequencies which swamped the Johnson noise.

VI. SUMMARY

We have studied the nonlinear dc conductivity behavior of two disordered systems, Ge-Au and C-Cu, on the metallic side of the metal-insulator transition for 1.3 K $< T <$ 4.2 K and $E <$ 500 V/cm. Analyzing dc conductivity versus dc E-field data within an electron-heating model yields unphysically long electron-phonon relaxation times. By stopping McMillan's renormalization process at a length scale where the electron wave packet gains an energy from the electric field E which is on the order of the potential fluctuations on that length scale we can simply extract the observed behavior. This model implies that the system achieves a steady state of classically diffusing particles.

ACKNOWLEDGMENTS

We wish to thank C. Yu and Y. Fu for many insightful discussions and D. Van Harlingen, G. Hilton, and R. Wakai for instruction in microlithography techniques. This work was supported by the National Science Foundation (NSF) under Contract No. NSF-DMR-83-16981. Samples were prepared in the microfabrication facility of the Materials Research Laboratory of the University of Illinois at Urbana-Champaign. Sample characterization was carried out in the Center for Microanalysis of Materials, University of Illinois at Urbana-Champaign, which is supported by U.S. Department of Energy under Contract No. DE-AC02-76ER01198. The work of J.M.M. was supported by the NSF under Grant No. NSF-DMR-86-12860. J.B.B. was supported by the Schlumberger Foundation.

*Present address: Naval Research Laboratory, 4555 Overlook Ave. SW, Washington, D.C. 20375-5000.

[1]G. J. Dolan and D. D. Osheroff, Phys. Rev. Lett. **43**, 721 (1979).

[2]D. J. Bishop, D. C. Tsui, and R. C. Dynes, Phys. Rev. Lett. **44**, 1153 (1980); D. J. Bishop, R. C. Dynes, and D. C. Tsui, Phys. Rev. B **26**, 773 (1982).

[3]H. Hoffmann, F. Hofmann, and W. Schoepe, Phys. Rev. B **25**, 5563 (1982).

[4]G. Bergmann, Z. Phys. B **49**, 133 (1982).

[5]S. I. Dorozhkin and V. T. Dolgopolov, Pis'ma Zh. Eksp. Teor. Fiz. **36**, 15 (1982) [JETP Lett. **36**, 18 (1982)].

[6]P. W. Anderson, E. Abrahams, and T. V. Ramakrishnan, Phys. Rev. Lett. **43**, 718 (1979).

[7]W. L. McMillan, Phys. Rev. B **24**, 2739 (1981).

[8]A. C. Anderson (private communication).

[9]M. Osofsky, Ph.D. thesis, University of Illinois at Urbana-Champaign, 1987.

[10]N. W. Ashcroft and N. D. Mermin, *Solid State Physics* (Holt, Rinehart and Winston, New York, 1976).

[11]M. L. Roukes, M. R. Freeman, R. B. Germain, and R. C. Richardson, Phys. Rev. Lett. **55**, 422 (1985).

[12]H. Tardy, Ph.D. thesis, University of Illinois at Urbana-Champaign, 1985.

[13]W. L. McMillan and J. M. Mochel, Phys. Rev. Lett. **46**, 556 (1981).

[14]G. Hertel, D. J. Bishop, E. G. Spencer, J. M. Rowell, and R. C. Dynes, Phys. Rev. Lett. **50**, 743 (1983).

[15]R. W. Cochrane and J. O. Strom-Olson, Phys. Rev. B **29**, 1088 (1984).

[16]J. Lesueur, L. Dumoulin, and P. Nedellec, Phys. Rev. Lett. **55**, 2355 (1985).

[17]T. Tsuzuki, Physica B+C **107B**, 679 (1981).

[18]M. Kaveh, M. J. Uren, R. A. Davies, and M. Pepper, J. Phys. C **14**, 413 (1981); N. F. Mott and M. Kaveh, *ibid.* **14**, L659 (1981).

[19]B. L. Altshuler and A. G. Aronov, Pis'ma Zh. Eksp. Teor. Fiz. **30**, 514 (1979) [JETP Lett. **30**, 482 (1979)].

[20]C. Yu and Y. Fu (private communication).

[21]E. Abrahams, P. W. Anderson, D. C. Licciardello, and T. V. Ramakrishnan, Phys. Rev. Lett. **42**, 673 (1979).

[22]Y. Fu, Phys. Rev. Lett. **60**, 345 (1988).